

# Searching Heavily Obscured Post-AGB Stars and Planetary Nebulae

## I. IRAS Candidates with 2MASS PSC Counterparts

G. Ramos-Larios<sup>1</sup>, M.A. Guerrero<sup>1</sup>, O. Suárez<sup>1,2</sup>, L.F. Miranda<sup>1</sup>, and J.F. Gómez<sup>1</sup>

<sup>1</sup> Instituto de Astrofísica de Andalucía, CSIC. c/Camino Bajo de Huétor 50, E-18008 Granada, Spain  
e-mail: gerardo@iaa.es\*, mar@iaa.es, lfm@iaa.es, jfg@iaa.es

<sup>2</sup> UMR 6525 H. Fizeau, Université de Nice Sophia Antipolis, CNRS, OCA. Parc Valrose, F-06108 Nice Cedex 2, France  
e-mail: olga.suarez@unice.fr

### ABSTRACT

**Context.** The transition from the Asymptotic Giant Branch (AGB) to the planetary nebula (PN) phase is critical in the shaping of PNe. It is suggested that the most asymmetric PNe are the descendant of massive AGB stars. Since these AGB stars are believed to evolve into heavily obscured post-AGB stars and PNe, the compilation of a sample of bona fide obscured post-AGB stars and PNe is important to help understand the formation of asymmetric PNe.

**Aims.** We aim to identify and characterize in the IR a large number of post-AGB stars and PNe and to assess their degree of optical obscuration. The improved positions will enable future detailed studies to determine their true nature, whereas the optical and IR properties can be used to investigate their spectral behaviour.

**Methods.** We have used 2MASS, *Spitzer* GLIMPSE, MSX, and *IRAS* data in search of the near-IR counterparts of a sample of 165 presumably obscured *IRAS* post-AGB and PN candidates, and DSS red images to identify the optical counterparts among the objects detected in the near-IR. The IR spectral energy distributions (SEDs) in the wavelength range from 1  $\mu\text{m}$  to 100  $\mu\text{m}$  of the sources with unambiguous near-IR counterparts have been analyzed using appropriate colour-colour diagrams.

**Results.** We have identified the near-IR counterparts of 119 sources out of the 165 *IRAS* post-AGB and PN candidates in our sample. The improved astrometric coordinates of these sources have allowed us to find optical counterparts for 59 of them, yielding a reduced sample of 60 optically obscured post-AGB star and PN candidates. Among the 119 sources with near-IR counterparts, only 80 have unambiguous identifications in the 2MASS Point Source Catalogue. For these sources, we find that objects with and without optical counterpart, while having similar mid- and far-IR colours, are segregated in colour-colour diagrams that use the near-IR *J* band to compute one of the colours.

**Key words.** stars: AGB and post-AGB – stars: evolution – planetary nebulae: general

### 1. Introduction

Stars of low- and intermediate-mass ( $0.8 - 1 M_{\odot} < M_i < 8 - 10 M_{\odot}$ ) experience heavy mass loss episodes during the red giant phase that subsequently intensify at the tip of the asymptotic giant branch (AGB). With typical mass loss rates  $10^{-4} - 10^{-5} M_{\odot} \text{ yr}^{-1}$ , the AGB wind ejects most of the stellar envelope in a short time, and the star enters the post-AGB phase, from which it evolves into a planetary nebula (PN). The study of objects in the post-AGB phase, the short transition from the AGB to the PN phase, is essential to understand the transformation of a spherically symmetric AGB envelope to an aspherical PN.

Objects in the transition from the AGB to the PN phase are strong far-infrared emitters, making them easily detectable by the *Infrared Astronomical Satellite* (*IRAS*). Furthermore, they are located in the [12]–[25] vs. [25]–[60] *IRAS* two-colour diagram in a well-defined region (van der Veen & Habing 1988). Therefore, the use of the *IRAS* two-colour diagram provides an invaluable strategy that has resulted in a number of catalogues of young PNe and their im-

mediate precursors, post-AGB stars (e.g. Preite-Martínez 1988; Pottasch et al. 1988; van der Veen et al. 1989; Ratag et al. 1990; Hu et al. 1993; Pereira & Miranda 2007). Recently, Suárez et al. (2006) presented a comprehensive optical spectroscopic atlas of post-AGB stars and young PNe selected from the *IRAS* Point Source Catalogue. In this work, a number of post-AGB candidates were so heavily obscured that no optical counterparts were found, while some others were not observed because they showed signs of strong obscuration in the optical.

Heavily obscured post-AGB stars and PNe represent objects whose circumstellar envelopes have not expanded enough to become optically thin. These objects may descend from the most massive AGB stars, as these are expected to be surrounded by very thick circumstellar envelopes during an important part or all the post-AGB evolution as a result of the large amounts of mass ejected in their envelopes (up to  $\sim 6 M_{\odot}$  for a star with initial mass  $7 M_{\odot}$ , Bloecker 1995). Moreover, the rapid evolution of the most massive post-AGB stars do not provide sufficient time for the circumstellar envelope to expand and become optically thin. Evidences of this evolutionary path are pro-

\* Postdoctoral Research Fellow

vided by young PNe whose very thick envelopes result in extremely high internal extinctions that prevent their detection in the optical (e.g., IRAS 15103–5754, van de Steene & Pottasch 1993; Suárez et al. 2006). Obscured post-AGB stars might be key objects to understand the late evolution of the most massive PN progenitors.

With this work, we start a program devoted to search heavily obscured post-AGB stars and PNe and to characterize them in the IR. The observational material includes data available in the 2MASS database, the *MSX* catalogue, and the *Spitzer* Space Telescope GLIMPSE Galactic plane survey, as well as recently acquired more sensitive, higher resolution near-IR observations. In this paper, the first in a series, we use 2MASS, *MSX*, and *Spitzer* GLIMPSE data to search for near-IR counterparts of presumably obscured *IRAS* post-AGB star and PN candidates. The accurate location of the sources with 2MASS counterparts has allowed us to determine whether these sources are really obscured in the optical or not. The 2MASS, *MSX*, and *Spitzer* GLIMPSE data have been further used to characterize the near and mid-IR properties of the sources with 2MASS counterparts, allowing us to derive their spectral energy distributions (SED) in the IR domain. In a second paper, we will present new, high-quality near-IR *JHK* observations in order to search for the near-IR counterparts of the faintest objects, to find the near-IR counterparts of the objects not resolved by 2MASS, to describe the morphology of sources with extended emission, and to investigate the variability of the objects with 2MASS counterparts.

The sample and archival data used in this paper are presented in §2 and §3, respectively. The identification of the *IRAS* sources with their 2MASS counterparts is described in §4, and their spectral properties are discussed in §5. Finally, a short summary is given in §6.

## 2. The Sample

The sample of *IRAS* post-AGB star and PN candidates investigated in this work is formed by the objects without optical counterpart in the sample of Suárez et al. (2006), as well as by objects included in the original sample of these authors but not observed because they showed strong indications of heavy obscuration. These *IRAS* sources fulfill the criteria used by Suárez et al. (2006) in order to select objects with a dust temperature in their envelopes of 80–200 K and an expanding radius of 0.01–0.1 pc. These selection criteria are:

- (i) The sources are well detected at 25 and 60  $\mu\text{m}$  in the *IRAS* Point Source Catalogue (see Beichman et al. 1988). The flux quality for each band must be:

$$\text{FQUAL} (12 \mu\text{m}) \geq 1;$$

$$\text{FQUAL} (25 \mu\text{m}) = 3;$$

$$\text{FQUAL} (60 \mu\text{m}) = 3.$$

- (ii) The ratios between the *IRAS* photometric fluxes satisfy the following conditions:

$$\frac{F_\nu (12 \mu\text{m})}{F_\nu (25 \mu\text{m})} \leq 0.50;$$

$$\frac{F_\nu (25 \mu\text{m})}{F_\nu (60 \mu\text{m})} \geq 0.35.$$

- (iii) For sources well detected at 100  $\mu\text{m}$  in the *IRAS* Point Source Catalogue (FQUAL (100  $\mu\text{m}$ )=3), it is further imposed:

$$\frac{F_\nu (60 \mu\text{m})}{F_\nu (100 \mu\text{m})} \geq 0.60.$$

- (iv) The sources must show a low *IRAS* variability index:

$$\text{VAR} \leq 60\%$$

The region of the *IRAS* two-colour diagram defined by the previous selection criteria has a small overlap with objects of different nature, mostly young stellar objects, OH stars, symbiotic stars, compact H II regions, and Seyfert galaxies. In particular, the IR SEDs, and thus the IR colours, of the circumstellar material around young stellar objects (e.g. Kenyon & Hartmann 1995) are very similar to those of post-AGB stars and young PNe, making it difficult to discern the nature of nebulae around young and evolved objects. On the contrary, Herbig Ae/Be stars, that exhibit distinct double-peak IR SEDs and are optically bright (e.g. Malfait et al. 1998; Meeus et al. 2001), are not easily mistaken for post-AGB stars and young PNe. To minimize the number of young stellar objects in the sample, two additional criteria have been imposed to our sample:

- (v) The sources are not classified in SIMBAD as young stars.
- (vi) The sources are not located near the boundary of known star forming regions.

With this criteria, the sample of *IRAS* post-AGB star and young PN candidates being presumably obscured sources consists of the 165 objects listed in Table 1. This table includes the *IRAS* names, coordinates, and error-ellipse (semi-major and semi-minor axes and position angle of the major axis) of these objects, together with their fluxes and flux quality factors in the *IRAS* 12  $\mu\text{m}$ , 25  $\mu\text{m}$ , 60  $\mu\text{m}$ , and 100  $\mu\text{m}$  bands. The typical accuracy of the coordinates of the *IRAS* sources is  $\sim 25''$ , ranging from  $\sim 10''$  up to  $45''$  for the objects in Tab. 1. The uncertainty in the *IRAS* coordinates is typically greater along the East-West direction. The location of these objects in the *IRAS* two-colour diagram is illustrated in Figure 1.

Some of the objects listed in Tab. 1 have been included in previous studies. High-quality images or detailed studies are available for IRAS 15452–5459 (Sahai et al. 2007), IRAS 17150–3224 (the Cotton Candy Nebula, Kwok, Su, & Hrivnak 1998; Hrivnak et al. 2006), IRAS 13356–6249, IRAS 13529–5934, IRAS 15144–5812, IRAS 17009–4154, and IRAS 17088–4221 (van de Steene et al. 2000), and IRAS 17516–2525 and IRAS 18135–1456 (Siódmiak et al. 2008). Near-IR photometric observations of IRAS 17404–2713, IRAS 17487–1922, IRAS 17516–2525, IRAS 18071–1727, and IRAS 19374+2359 (van der Veen et al. 1989), and spectroscopic observations of IRAS 17540–2753 and IRAS 18135–1456 (Oudmaijer et al. 1995) have also been reported.

## 3. Archival Data

In order to identify and characterize the near- and mid-IR counterparts of the *IRAS* candidates to post-AGB stars and PNe in our sample, we have searched available 2MASS,

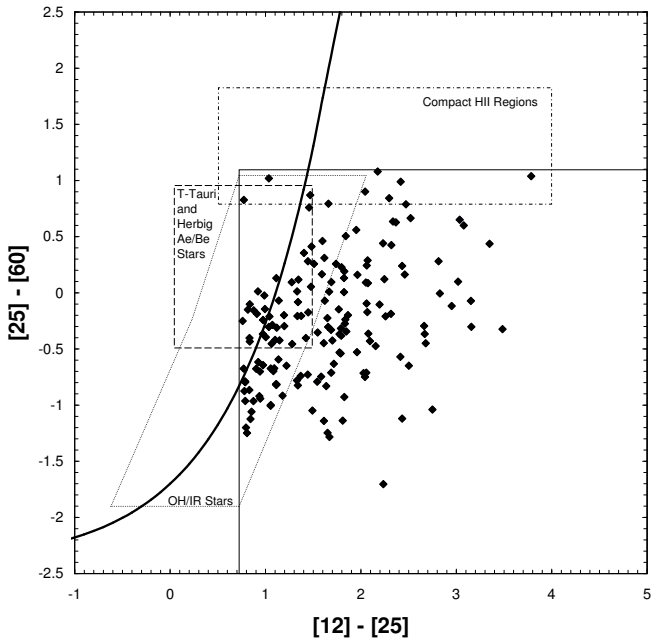


**Fig. 1.** *IRAS* colour-colour diagram showing the location of the *IRAS* sources in our sample. The thin solid lines represent our selection criteria, while the solid thick line represents the expected colours for AGB stars (Bedijn 1987). The loci of OH/IR stars (Sivagnaman 1989; te Lintel Hekkert et al. 1991), T-Tauri and Herbig Ae/Be stars (Harris, Clegg, & Hughes 1988), and compact H II regions (Antonopoulos & Pottasch 1987) that overlap with post-AGB stars and PNe are also overlaid on the diagram. *IRAS* colours are computed as  $[A]-[B]=2.5 \log(F_\nu(B)/F_\nu(A))$ .

*MSX*, and *Spitzer* GLIMPSE data products. The different properties of these catalogues are described below.

The 2 Microns All Sky Survey (2MASS) provides images of the complete sky in the  $J$  ( $1.25\text{ }\mu\text{m}$ ),  $H$  ( $1.65\text{ }\mu\text{m}$ ), and  $K_S$  ( $2.17\text{ }\mu\text{m}$ ) bands (Skrutskie et al. 2006). The image pixel scale is  $1''$  and the typical spatial resolution in the survey was  $\sim 5''$ , as derived from the FWHM of the stars in the images. The  $10\sigma$  detection limit for point-sources is  $J < 15.8$  mag,  $H < 15.1$  mag, and  $K_S < 14.3$  mag.

The Mid-course Space Experiment (*MSX*) provides a detailed mid-IR map of a narrow strip,  $|b| \leq 5^\circ$ , of the whole Galactic plane in four different bands, namely band A ( $8.28\text{ }\mu\text{m}$ ), C ( $12.13\text{ }\mu\text{m}$ ), D ( $14.65\text{ }\mu\text{m}$ ), and E ( $21.3\text{ }\mu\text{m}$ ). The positional uncertainty in the *MSX* Point Source Catalogue (MSX6C) is of the order of  $2''$ , while the spatial resolution is quoted to be  $18''.3$  (Price et al. 2001). The sensitivity levels for the bands A, C, D and E are 160 mJy, 1200 mJy, 1000 mJy and 3000 mJy respectively.

The Galactic Legacy Infrared Midplane Survey Extraordinaire (GLIMPSE) project obtained *Spitzer* Infrared Array Camera (IRAC) observations of the Galactic plane within the latitude and longitude ranges  $|b| \leq 1^\circ$ , and  $|l| = 10^\circ - 65^\circ$ , respectively, in four bands with wavelengths (and bandwidths)  $3.550\text{ }\mu\text{m}$  ( $0.75\text{ }\mu\text{m}$ ),  $4.493\text{ }\mu\text{m}$  ( $1.9015\text{ }\mu\text{m}$ ),  $5.731\text{ }\mu\text{m}$  ( $1.425\text{ }\mu\text{m}$ ), and  $7.872\text{ }\mu\text{m}$  ( $2.905\text{ }\mu\text{m}$ ). These results were subsequently processed to yield the GLIMPSE Image Atlas with a pointing accuracy of  $\sim 0''.3$ , and a spatial resolution that varies between  $1''.7$  and  $2''.0$  (Fazio et al. 2004). The sensitivity (saturation levels) for the different bands are 0.5 mJy (439 mJy) in the  $3.6\text{ }\mu\text{m}$  band, 0.5 mJy (450 mJy) in the  $4.5\text{ }\mu\text{m}$  band, 2 mJy (2930 mJy) in the  $5.8\text{ }\mu\text{m}$  band, and 5 mJy (1590 mJy) in the  $8.0\text{ }\mu\text{m}$  band.

#### 4. Source Identification

The accuracy of the coordinates of an *IRAS* source may not be good enough to allow a straightforward identification of its counterpart in the 2MASS, *MSX* or GLIMPSE catalogues. This is especially the case of *IRAS* sources in crowded fields located along the Galactic plane or near the Galactic Center, for which the error-ellipse typically includes several near-IR sources. In order to define a strategy to search for the near- and mid-IR counterparts of the *IRAS* sources in Tab. 1, a comparison between the three databases used in this work can be useful.

The 2MASS images provide a complete coverage of the sky with a spatial resolution ( $\sim 5''$ ) better than the positional uncertainty of the *IRAS* sources in Tab. 1. However, the sensitivity of the 2MASS images to obscured sources is limited because of the large extinction and intrinsic red colours of these sources. Accordingly, the identification of the 2MASS counterparts of the *IRAS* sources in our sample is not obvious in general. This is not the case of the GLIMPSE Image Atlas that has a high sensitivity to mid-IR sources and provides better spatial resolution ( $\leq 2''.0$ ) than the *MSX* and 2MASS images. This database thus seems especially suited to determine with a great accuracy the position of the *IRAS* sources in Tab. 1. Unfortunately, its limited spatial coverage results in a reduced number of sources with available GLIMPSE data. On the other hand, the *MSX* data have an extremely good sensitivity to obscured sources and its coverage is sufficiently good to include a significant fraction of the sources in our sample. The *MSX* images, however, have a poor spatial resolution ( $\sim 18''$ ) that can make difficult to pinpoint the near-IR counterpart.

Given the different properties of the 2MASS, *MSX*, and GLIMPSE Image Atlas, we have proceeded as follows in order to identify the near-IR counterparts of the *IRAS* sources. When available, we have first examined the GLIMPSE images to pinpoint the accurate location of the *IRAS* sources, thus allowing us to find its near-IR counterpart in 2MASS images. This procedure is illustrated in Figure 2 for *IRAS* 17359–2902; the bright *Spitzer* mid-IR source inside its *IRAS* error-ellipse allows the unambiguous identification of its near-IR counterpart among the near-IR sources within this ellipse in the 2MASS image. The use of the GLIMPSE images resulted in the identification of the near-IR counterparts of 22 sources in Tab. 1, although it must be noticed that some heavily obscured *Spitzer* sources were not detected in the 2MASS images and are not listed in Tab. 1. We then examined the *MSX* data of the sources with no GLIMPSE data available and were able to find the near-IR counterparts for 52 additional sources in Tab. 1. A typical example of the identification of the near-IR counterpart of an *IRAS* source using *MSX* data is shown in Figure 2 for *IRAS* 17010–3810; the position of the *MSX* source MSX6C G347.4963+01.8505, coincident within  $1''$  with the position of the source 2MASS 17042731–3814417 (marked in the 2MASS image), has allowed us to determine that this is the near-IR counterpart of *IRAS* 17010–3810. Finally, we have examined the *JHK* 2MASS images of the *IRAS* sources with no GLIMPSE and *MSX* data available,

and selected the near-IR counterparts that appear as isolated sources within the error-ellipse of the *IRAS* source and whose near-IR colours are typical of post-AGB stars or PNe, i.e.,  $(J - H) \sim 1.0$  and  $(H - K) \sim 0.4$  (García-Lario et al. 1997). This has added an additional number of 43 *IRAS* sources with 2MASS counterparts. The result is a total of 119 sources with near-IR emission out of the sample of 165 sources listed in Tab. 1.

Among these 119 *IRAS* sources detected in the near-IR, there are 80 sources with a reliable counterpart in the 2MASS Point Source Catalogue (PSC). The remaining 39 *IRAS* sources in Tab. 1 have near-IR emission detected in 2MASS, but the assignation of a counterpart in the 2MASS PSC is dubious due either to their extended appearance in the 2MASS images, to the possible contamination by an adjacent source, or to their extreme faintness, at the detection limit of 2MASS.

The sample of the 80 *IRAS* post-AGB and PN candidates in Tab. 1 with a counterpart in the 2MASS PSC is listed in Table 2 with their coordinates and near-IR magnitudes, and their identification charts are shown in Figure 3. The angular separation with the position of the *IRAS* source is also listed in this table. The distance between the *IRAS* and 2MASS coordinates is typically below  $5''$ , i.e., within the ellipse-error of the *IRAS* coordinates, with no preferential direction of the distance vector. In a few cases, the offset between the *IRAS* and 2MASS coordinates is larger than the *IRAS* coordinates uncertainty. Obviously, these are sources that have been identified through their GLIMPSE *Spitzer* or *MSX* images. A close inspection to the original *IRAS* images reveals that these sources are either extended sources or multiple, unresolved sources, thus introducing a significant offset in their *IRAS* coordinates.

The sample of the 39 *IRAS* post-AGB and PN candidates in Tab. 1 with a 2MASS counterpart but dubious assignation in the 2MASS PSC are listed in Table 3 and their identification charts are shown in Figure. 4.

Finally, the 46 sources that do not have a 2MASS counterpart are listed in Table 4. Most of these sources have been observed by *MSX* and many of them have even *Spitzer* GLIMPSE observations, but no near-IR counterpart is detected in 2MASS at the improved astrometric positions provided by the *MSX* and *Spitzer* GLIMPSE catalogues. Only IRAS 16245–3859, IRAS 18385+1350, and IRAS 21537+6435 have no *Spitzer* GLIMPSE nor *MSX* observations, and they do not have an obvious near-IR counterpart in 2MASS images within their *IRAS* ellipse-error. The study of sources in Tab. 3 and 4 requires near-IR observations of greater spatial resolution and sensitivity, respectively, than the 2MASS observations used in this paper. These observations will be presented in a subsequent paper.

## 5. Discussion

### 5.1. Degree of Obscuration Among the IRAS Sources

Using the improved accuracy of the 2MASS coordinates, we have searched for the optical counterpart of the sources in Tab. 2 and 3 in the red plates of the Digitized Sky Survey<sup>1</sup> (DSS). The information on the optical detection of these

sources, added to Tab. 2 and 3, unveils a significant population of optical counterparts for the a priori supposedly heavily obscured *IRAS* post-AGB and PN candidates. Out of the 119 objects with 2MASS counterpart, 59 have an optical counterpart, i.e., only 50% of the objects in these two tables can be considered optically obscured.

Despite the limited spatial resolution and sensitivity of the 2MASS images and, very notably, of the DSS red images, the homogeneity of these two databases grants a brightness limited search that is meaningful for a statistical analysis. Therefore, the simple detection of an *IRAS* source in our sample in the DSS and/or 2MASS images allows us to determine the degree of obscuration of this source. Accordingly, we can define three types of sources based on the shortest wavelength at which they are detected:

- Type *m* sources (for mid-IR): Heavily obscured sources that are neither detected in DSS red images, nor in the 2MASS images.
- Type *n* sources (for near-IR): Optically obscured sources detected in 2MASS images, but not in DSS images.
- Type *o* sources (for optical): Sources with little optical and near-IR obscuration detected both in DSS and 2MASS images.

Type *m* sources will be found among the sources listed in Tab. 4. The study of these sources will be postponed to an upcoming paper. Similarly, the 2MASS spatial resolution has not allowed us to measure the *JHK* magnitudes of sources in Tab. 3 and the study of this sources will also be deferred. In the following, we will focus on the sources listed in Tab. 2, i.e., the sources of types *n* and *o* with a near-IR counterpart in the 2MASS PSC.

### 5.2. Spectral Properties

The near- and mid-IR properties of the type *o* and type *n* sources can be used to investigate their nature. Using the *JHK* magnitudes of the sources listed in Tab. 2, the *MSX* and *Spitzer* GLIMPSE fluxes given in Table 5, and their *IRAS* fluxes (Tab. 1), we have built the IR spectral energy distributions (SEDs) that are shown in Fig. 3. The analysis of the IR SEDs of these sources can be performed by studying the different colour diagrams shown in Figures 5, 6, and 7.

The  $J - H$  vs.  $H - K_s$  colour diagram (Fig. 5) shows that the sources in this sample have near-IR colours mostly in the ranges  $0.5 < J - H < 3$  and  $0.2 < H - K_s < 3$ , although a few sources are very highly obscured, with  $H - K_s$  colours up to  $\sim 5$  mag. In this diagram, sources detected in the optical tend to have smaller values of their  $J - H$  and  $H - K_s$  colours, with almost all these sources having  $J - H < 1.6$  and  $H - K_s < 1.4$ . This trend is more clearly seen in the  $J - K_s$  vs.  $H$  diagram (Fig. 5) that shows noticeable differences

the UK Science and Engineering Research Council, until 1988 June, and thereafter by the Anglo-Australian Observatory. The Palomar Observatory Sky Survey was funded by the National Geographic Society. The Oschin Schmidt Telescope is operated by the California Institute of Technology and Palomar Observatory. The plates were processed into the present compressed digital form with the permission of these institutes. The Digitized Sky Survey was produced at the Space Telescope Science Institute under US government grant NAGW-2166.

<sup>1</sup> The Digitized Sky Survey is based on photographic data obtained using the UK Schmidt Telescope and the Oschin Schmidt Telescope on Palomar Mountain. The UK Schmidt was operated by the Royal Observatory of Edinburgh, with funding from

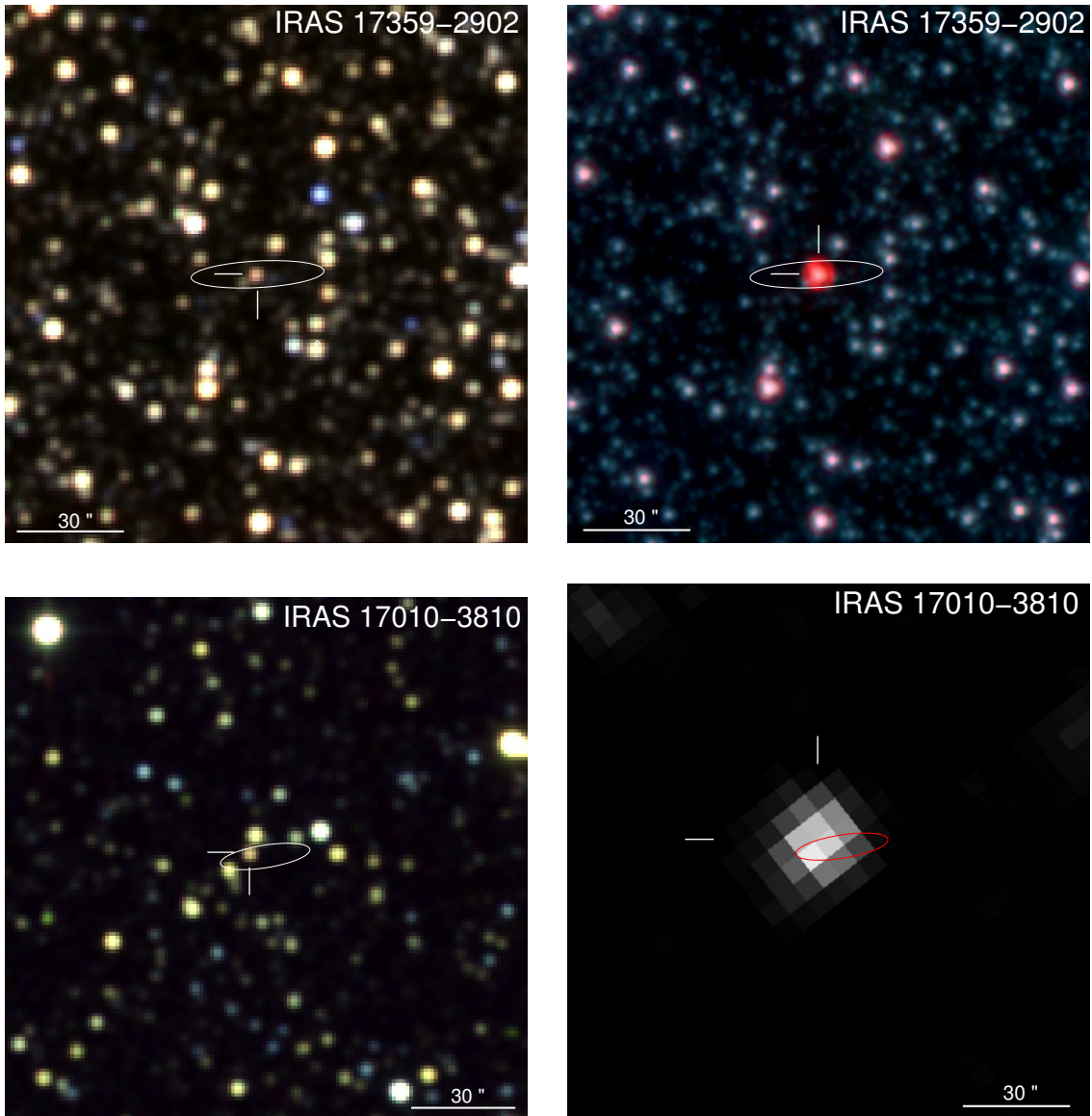


**Fig. 2.** Representative examples of objects whose near-IR counterparts have been identified using *Spitzer* GLIMPSE or *MSX* data. (top) 2MASS  $J$  (blue),  $H$  (green), and  $K_s$  (red) composite picture (left) and *Spitzer* GLIMPSE 3.6  $\mu\text{m}$  (blue), 4.5  $\mu\text{m}$  (green), and 8.0  $\mu\text{m}$  (red) composite picture (right) of IRAS 17359–2902. (bottom) 2MASS  $J$  (blue),  $H$  (green), and  $K_s$  (red) composite picture (left) and *MSX* image in the 8.28  $\mu\text{m}$  A band (right) of IRAS 17010–3810. The locations of the near-IR counterparts and the *IRAS* ellipse-error are overlaid. North is up, east to the left.

in the distribution of sources of types  $o$  and  $n$ ; type  $o$  sources are mostly located on the band  $1 < J - K_s < 2.5$ , while type  $n$  sources are located mostly above this band, with  $J - K_s \geq 2.5$ . The interpretation of this behaviour is clearly illustrated by the SED of these two types of sources: type  $o$  sources use to have flat or shallow near-IR SEDs (e.g., IRAS 14521–5300), while type  $n$  sources usually present steep near-IR SEDs (e.g., IRAS 14104–5819).

The segregation between the sources of type  $o$  and  $n$  with 2MASS PSC counterpart is also clear in the *MSX-J* colour diagram (Fig. 6). In this diagram, sources of type  $o$  have  $J-[8.3]$  colours typically lower than 10. On the contrary, sources of type  $o$  and  $n$  are not separated in the *MSX* colour-colour diagram (Fig. 6) on which both types are spread over a wide region. Interestingly, these sources are mostly located in the quadrants of this diagram that have been suggested to be populated by AGB and post-AGB

stars, while generally avoiding the quadrant on which objects in star forming regions are typically found (Sevenster 2002). This result confirms our selection criteria for AGB and post-AGB stars in §2.

Similarly, the *IRAS* colour-colour diagram shown in Fig. 7 does not single out the optical type  $o$  sources from the near-IR type  $n$  sources in Tab. 2. On the other hand, the two types of sources show different properties in the  $K_s-[8.3]$  vs.  $J-[25]$  colour-colour diagram (Fig. 7). In this diagram (spotlighted by Suárez et al., in prep., as able to discriminate very efficiently between different types of SEDs of post-AGB stars), sources of type  $o$  have mostly  $J-[25] < 7$  and sources of type  $n$  have  $J-[25] > 9.6$ , with an intermediate region populated by both type  $o$  and  $n$  sources. It is interesting to note that the  $K_s-[8.3]$  and  $J-[25]$  colours of the sources in our sample are clearly correlated.

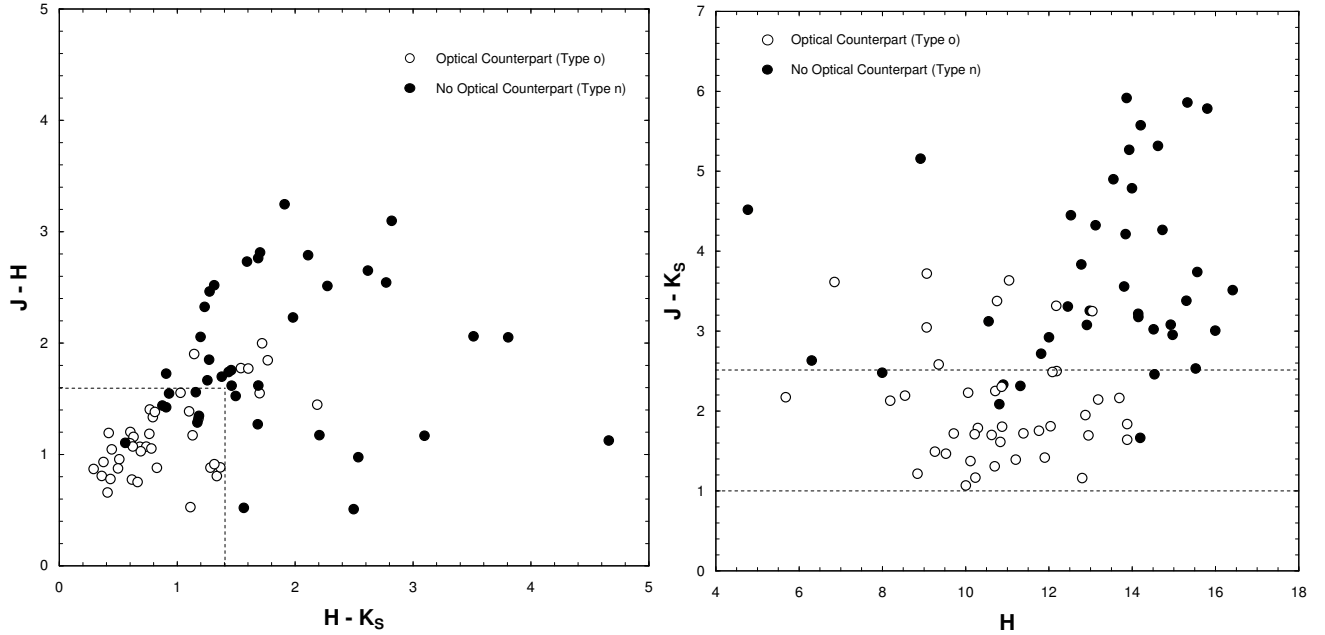


**Fig. 5.** (left)  $J - H$  vs.  $H - K_s$  and (right)  $J - K_s$  vs.  $H$  2MASS diagrams of the *IRAS* post-AGB star and PN candidates in our sample with 2MASS PSC counterparts. The dashed lines mark the regions mostly occupied by sources of type *o* (sources with optical counterpart).

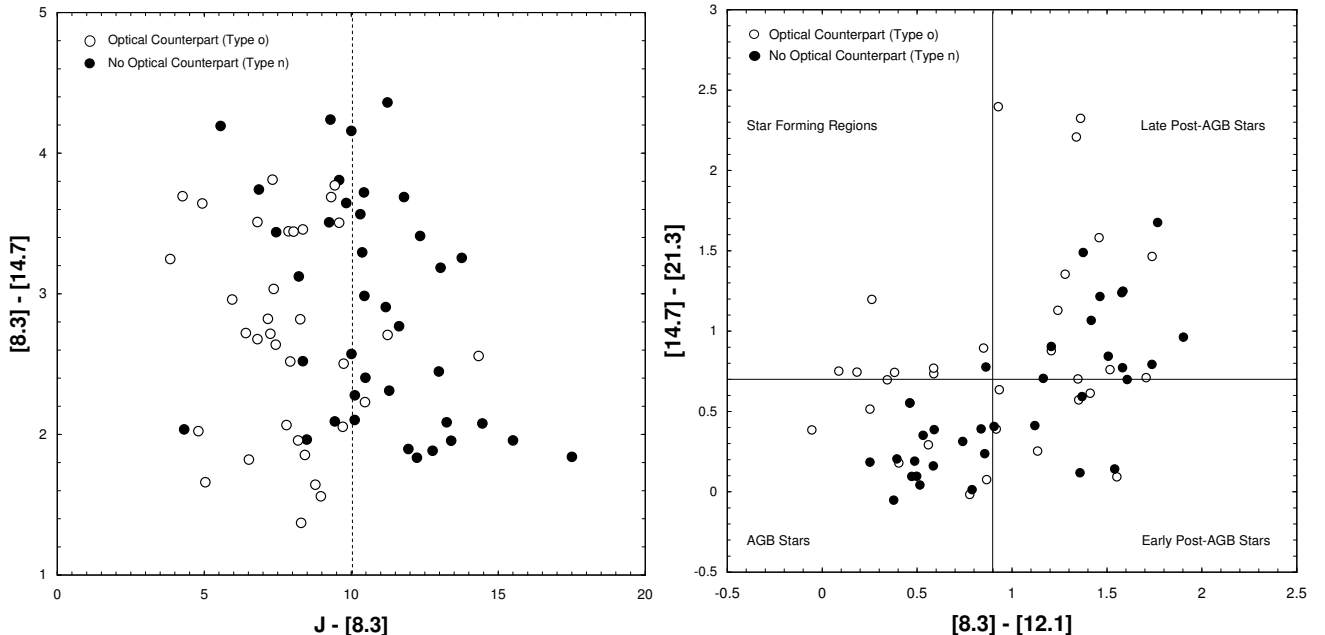


**Fig. 6.** (left) MSX- $J$  and (right) MSX colour-colour diagrams of the *IRAS* post-AGB star and PN candidates with 2MASS PSC and MSX counterparts. The vertical line in the MSX- $J$  colour-colour diagram at  $J - [8.3] = 10$  marks a rough division between sources of type *o* and *n*. The vertical and horizontal lines in the MSX colour-colour diagram divide it into four quadrants that correspond to areas of higher probability of containing the different types of objects labeled on the diagram (Sevenster 2002).

In all the colour-colour diagrams shown in Figs. 5, 6, and 7, the use of colours in which the  $J$  magnitude is involved has allowed us to separate the sources with optical counterpart from these obscured in the optical. It can be concluded that the relation between the magnitude in the  $J$  band and in different bands in the near-, mid-, and far-IR is critical in order to forecast the level of emission at optical wavelengths.

### 5.3. Sources in the Spitzer GLIMPSE Image Atlas

The *Spitzer* images of the *IRAS* post-AGB star and PN candidates with 2MASS PSC counterparts that are available in the GLIMPSE Image Atlas are presented in Figure 8. All *IRAS* sources identified in the *Spitzer* GLIMPSE Image Atlas are point-like, except IRAS 18229–1127, IRAS 18454+0001, and IRAS 18576+0341, whose PSFs have FWHMs broader

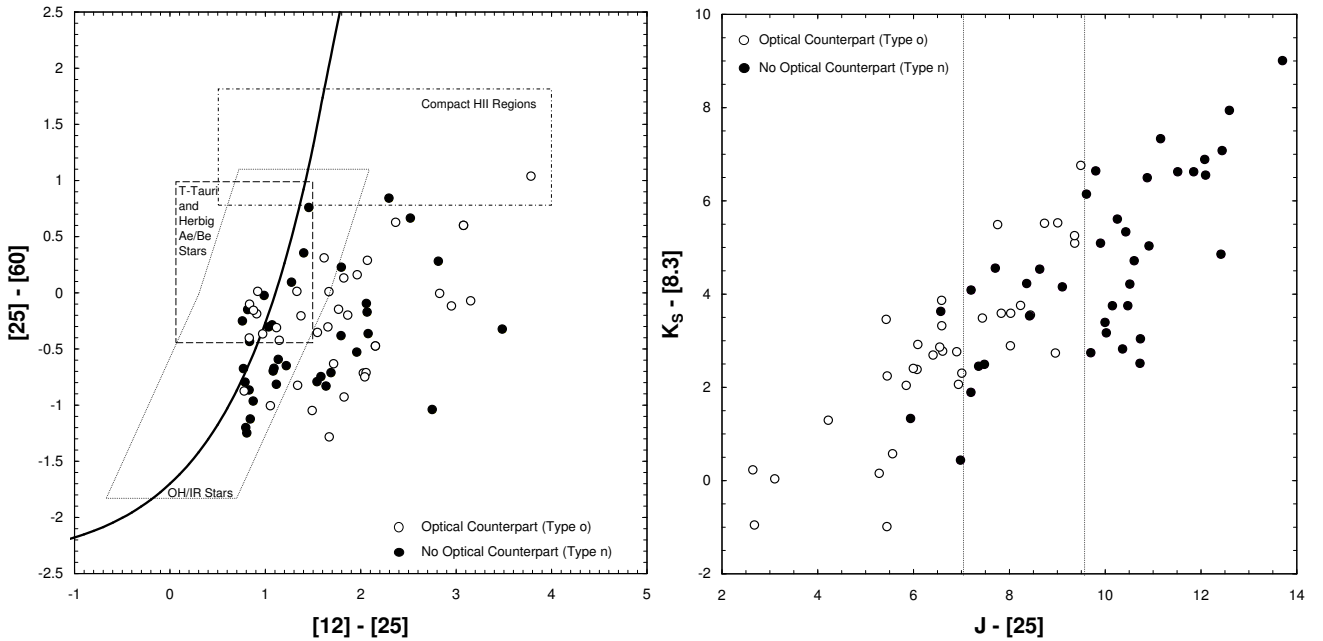


**Fig. 7.** (left) *IRAS* and (right)  $K_s - [8.3]$  vs.  $J - [25]$  colour-colour diagrams of the *IRAS* post-AGB star and PN candidates with 2MASS PSC and *MSX* counterparts. In the *IRAS* colour-colour diagram, the locii of OH/IR stars, T-Tauri and Herbig Ae/Be stars, and compact H II are overlaid as in Fig 1. The vertical lines in the  $K_s - [8.3]$  vs.  $J - [25]$  diagram mark three regions with the leftmost being dominated by sources with optical counterpart (type *o* sources), and the rightmost being exclusively populated by sources with no optical counterpart (type *n* sources).

than those of point sources in their respective images. IRAS 18229–1127 has a FWHM of  $3''.0$  in the 4 IRAC bands, just above the FWHM of stellar sources ( $\sim 2''.1$ ). IRAS 18454+0001 is a point-like source, except in the  $8\ \mu\text{m}$  band, with a FWHM of  $2''.4$  (compared to the FWHM of  $1''.9$  of stellar sources). Finally, IRAS 18576+0341 has the broadest FWHM,  $\sim 5''.0$  (the FWHM of stellar sources is  $\sim 2''.0$ ), in the  $3.6\ \mu\text{m}$ ,  $4.5\ \mu\text{m}$ , and  $5.8\ \mu\text{m}$  bands (its image in the  $8\ \mu\text{m}$  band is saturated).

## 6. Summary

Using 2MASS, *Spitzer* GLIMPSE, and *MSX* data products, we have identified 119 near-IR counterparts out of a sample of 165 *IRAS* post-AGB star and PN candidates. For these sources, we provide near-IR identification charts. Among these 119 sources with near-IR counterpart, 80 objects have unambiguous 2MASS PSC counterpart. For these sources, we further provide improved coordinates, and IR energy spectral distributions from  $1\ \mu\text{m}$  to  $100\ \mu\text{m}$ .

Using the improved coordinates of the sources with 2MASS PSC counterpart, we have searched for their optical counterparts in DSS red plates and found that  $\sim 50\%$  of these sources are detected in the optical. We have then investigated the different spectral properties of the sources with and without optical counterpart, dubbed sources of type *o* and *n*, respectively. The two types of sources have similar mid- and far-IR colours, but they appear clearly segregated in colour-colour diagrams in which the magnitude in the *J* band is used to compute one of the colours.

**Acknowledgements.** This publication makes use of data products from the 2MASS, which is a joint project of the University of Massachusetts and the Infrared Processing and Analysis Center/California Institute of Technology, funded by the National

Aeronautics and Space Administration and the National Science Foundation.

This work is based, in part, on observations made with the *Spitzer* Space Telescope, which is operated by the Jet Propulsion Laboratory, California Institute of Technology under a contract with NASA. Support for this work was provided by an award issued by JPL/Caltech. GRL acknowledges support of a postdoctoral fellowship from CONACyT (Mexico) grant 75861.

MAG, OS, LFM, and JFG acknowledge support from Consejería de Innovación, Ciencia y Empresa de Junta de Andalucía. GRL, MAG, and LFM are partially funded by grant AYA2005-01495 of the Spanish Ministerio de Educación y Ciencia (MEC). JFG is partially funded by grant 2005-08523-C03-03 of MEC. GRL, MAG, OS, and LFM are partially funded by grant AYA2008-01934 of the Spanish Ministerio de Ciencia e Innovación (MICINN). OS and JFG are partially funded by grant 2008-06189-C03-01 of MICINN.

This research has made use of the SIMBAD database, operated at CDS, Strasbourg, France.

## References

- Antonopoulos, E., & Pottasch, S.R. 1987, A&A, 173, 108
- Bedijn, P.J. 1987, A&A, 186, 136
- Beichman, C. A., Neugebauer, G., Habing, H. J., Clegg, P. E., & Chester, T. J. 1988, Infrared astronomical satellite (IRAS) catalogs and atlases. Volume 1: Explanatory supplement, 1,
- Benjamin, R. A., Churchwell, E., Babler, B. L., et al. 2003, PASP, 115, 953
- Bloecker, T. 1995, A&A, 299, 755
- Fazio, G. G., Hora, J. L., Allen, L. E., et al. 2004, ApJS, 154, 10
- García-Lario, P., Manchado, A., Pych, W., & Pottasch, S. R. 1997, A&AS, 126, 479
- García-Lario, P., Manchado, A., Suso, S. R., Pottasch, S. R., & Olling, R. 1990, A&AS, 82, 497
- Harris, S., Clegg, P., & Hughes, J. 1988, MNRAS, 235, 441
- Hrivnak, B. J., Kelly, D. M., Su, K. Y. L., Kwok, S., & Sahai, R. 2006, ApJ, 650, 237
- Hu, J. Y., Slijkhuis, S., de Jong, T., & Jiang, B. W. 1993, A&AS, 100, 413
- Kenyon, S. J., & Hartmann, L. 1995, ApJS, 101, 117
- Kwok, S., Su, K. Y. L., & Hrivnak, B. J. 1998, ApJ, 501, L117
- Malfait, K., Bogaert, E., & Waelkens, C. 1998, A&A, 331, 211

- Meeus, G., Waters, L. B. F. M., Bouwman, J., van den Ancker, M. E.,  
 Waelskens, C., & Malfait, K. 2001, A&A, 365, 476  
 Oudmaijer, R. D., Waters, L. B. F. M., van der Veen, W. E. C. J., &  
 Geballe, T. R. 1995, A&A, 299, 69  
 Pereira, C.B., & Miranda, L.F. 2007, A&A, 462, 231  
 Pottasch, S. R., Olling, R., Bignell, C., & Zijlstra, A. A. 1988, A&A,  
 205, 248  
 Preite-Martinez, A. 1988, A&AS, 76, 317  
 Price, S. D., Egan, M. P., Carey, S. J., Mizuno, D. R., & Kuchar,  
 T. A. 2001, AJ, 121, 2819  
 Ratag, M. A., Pottasch, S. R., Zijlstra, A. A., & Menzies, J. 1990,  
 A&A, 233, 181  
 Sahai, R., Morris, M., Sánchez Contreras, C., & Claussen, M. 2007,  
 AJ, 134, 2200  
 Sevenster, M.N. 2002, AJ, 123, 2772  
 Siódmiak, N., Meixner, M., Ueta, T., Sugerman, B. E. K., van de  
 Steene, G. C., & Szczepański, R. 2008, ApJ, 677, 382  
 Sivagnaman, P. 1989, Ph.D. Thesis, University of Paris VII, France  
 Skrutskie, M. F., Cutri, R. M., Stiening, R., et al. 2006, AJ, 131, 1163  
 Suárez, O., García-Lario, P., Manchado, A., Manteiga, M., Ulla, A.,  
 & Pottasch, S. R. 2006, A&A, 458, 173  
 te Lintel Hekkert, P., Caswell, J.L., Haynes, R.F., Norris, R.P., &  
 Habing, H.J. 1991, A&AS, 90, 327  
 van de Steene, G. C. M., & Pottasch, S.R. 1993, A&A, 274, 895  
 van de Steene, G. C. M., van Hoof, P. A. M., & Wood, P. R. 2000,  
 A&A, 362, 984  
 van der Veen, W. E. C. J., Habing, H. J., & Geballe, T. R. 1989,  
 A&A, 226, 108  
 van der Veen, W. E. C. J., & Habing, H. J. 1988, A&A, 194, 125

**Table 1.** IRAS Identifications, Positions and Fluxes of Post-AGB Star and PN Candidates.

Name	RA (J2000)	DEC (J2000)	Major Axis ( $\text{''}$ )	Minor Axis ( $\text{''}$ )	PA ( $^{\circ}$ )	$F_{12}$ [Jy]	$F_{25}$ [Jy]	$F_{60}$ [Jy]	$F_{100}$ [Jy]	FQUAL <sup>†</sup>
IRAS 00509+6623	00 54 07.7	+66 40 13	15	4	38	3.12	8.25	3.27	4.59	3 3 3 1
IRAS 04137+7016	04 19 08.8	+70 23 23	15	5	75	0.65	2.12	1.39	1.12	3 3 3 1
IRAS 05573+3156	06 00 33.4	+31 56 43	15	5	89	7.95	47.93	80.21	108.90	3 3 3 3
IRAS 06499+0145	06 52 29.9	+01 42 00	17	5	96	0.93	15.16	27.60	46.16	3 3 3 3
IRAS 08242–3828	08 26 03.5	–38 38 48	29	6	116	11.58	26.77	22.53	10.75	3 3 3 3
IRAS 08351–4634	08 36 45.8	–46 44 46	14	4	117	15.02	31.02	12.78	8.81	3 3 3 2
IRAS 09055–4629	09 07 19.4	–46 41 21	15	4	126	0.74	3.05	1.47	32.70	3 3 3 1
IRAS 09102–5101	09 11 53.5	–51 13 51	12	4	129	0.56	3.73	4.87	35.11	2 3 3 1
IRAS 09119–5150	09 13 32.9	–52 02 39	14	3	129	0.79	3.82	2.13	25.94	3 3 2 1
IRAS 09370–4826	09 38 53.3	–48 40 10	24	5	124	10.82	30.14	14.16	5.41	3 3 3 3
IRAS 09378–5117	09 39 36.9	–51 31 26	15	3	136	1.87	6.43	3.01	16.31	3 3 3 1
IRAS 09500–5236	09 51 49.5	–52 50 40	14	3	147	0.58	2.23	4.49	18.44	3 3 3 1
IRAS 10194–5625	10 21 15.2	–56 40 32	17	5	146	16.75	57.02	27.78	52.91	3 3 3 1
IRAS 11339–6004	11 36 21.0	–60 20 56	18	3	143	1.96	8.45	4.24	23.02	3 3 3 1
IRAS 11381–6401	11 40 32.3	–64 18 33	14	3	146	5.41	27.76	17.02	72.42	3 3 3 1
IRAS 11444–6150	11 46 54.0	–62 07 09	14	3	157	3.22	14.33	13.42	76.35	2 3 3 1
IRAS 11488–6432	11 51 17.0	–64 49 09	15	5	144	1.56	3.37	3.07	14.49	3 3 3 1
IRAS 11544–6408	11 56 57.2	–64 25 11	15	4	142	12.49	29.81	12.52	12.57	3 3 3 1
IRAS 11549–6225	11 57 30.8	–62 42 12	12	3	149	7.60	20.06	10.79	33.30	3 3 3 3
IRAS 12262–6417	12 29 04.2	–64 33 37	16	6	146	2.53	8.98	7.43	16.21	3 3 3 1
IRAS 12309–5928	12 33 44.8	–59 45 18	15	4	139	1.99	5.44	2.93	19.26	3 3 3 1
IRAS 12360–5740	12 38 53.2	–57 56 31	21	6	129	0.53	3.62	2.43	14.92	2 3 3 1
IRAS 12405–6219	12 43 31.1	–62 36 13	16	4	132	16.63	109.30	250.70	429.60	3 3 3 2
IRAS 13293–6000	13 32 38.4	–60 15 36	16	5	129	0.75	1.95	4.99	34.31	3 3 3 1
IRAS 13356–6249	13 39 05.8	–63 04 44	18	6	129	6.06	149.90	111.30	202.70	3 3 3 1
IRAS 13398–5951	13 43 12.2	–60 07 01	21	4	125	2.43	5.43	2.24	31.43	3 3 3 1
IRAS 13404–6059	13 43 52.8	–61 14 46	25	3	129	5.24	15.76	12.00	86.92	3 3 3 1
IRAS 13421–6125	13 45 34.9	–61 40 07	20	5	128	15.21	31.17	13.93	122.10	3 3 3 1
IRAS 13427–6531	13 46 25.7	–65 46 24	19	6	131	0.53	6.28	4.15	9.94	3 3 3 1
IRAS 13483–5905	13 51 44.1	–59 20 16	22	6	125	6.05	16.94	12.72	27.99	3 3 3 1
IRAS 13500–6106	13 53 34.5	–61 20 52	17	6	127	1.81	8.28	6.74	123.20	3 3 3 1
IRAS 13529–5934	13 56 24.8	–59 48 55	25	7	125	1.37	10.36	9.41	48.06	3 3 3 1
IRAS 14104–5819	14 14 00.4	–58 33 57	23	7	128	5.56	11.56	3.83	29.82	3 3 3 1
IRAS 14249–5310	14 28 24.9	–53 24 06	21	5	117	11.82	29.00	23.20	9.63	3 3 3 3
IRAS 14521–5300	14 55 45.9	–53 12 33	23	5	109	2.44	6.46	2.58	13.13	3 3 3 1
IRAS 15038–5533	15 07 35.4	–55 44 54	22	5	110	1.22	3.40	1.61	84.62	3 3 3 1
IRAS 15103–5754	15 14 18.9	–58 05 20	18	3	2	10.80	101.50	126.50	103.40	3 3 3 2
IRAS 15144–5812	15 18 22.0	–58 23 13	17	4	116	7.67	35.59	35.89	149.50	3 3 3 1
IRAS 15229–5433	15 26 42.3	–54 44 23	17	5	110	0.42	3.84	2.27	80.68	2 3 3 1
IRAS 15284–6026	15 32 37.1	–60 37 04	23	5	109	2.10	9.97	10.88	32.46	3 3 3 1
IRAS 15408–5657	15 44 48.1	–57 07 08	23	7	110	26.60	54.08	29.03	16.22	3 3 2 2
IRAS 15408–5413	15 44 39.9	–54 23 05	29	4	107	166.90	350.60	111.00	154.20	3 3 3 1
IRAS 15452–5459	15 49 11.5	–55 08 52	21	7	103	87.05	242.70	273.60	401.10	3 3 3 1
IRAS 15531–5704	15 57 10.4	–57 13 20	28	6	102	2.27	4.69	2.27	70.81	3 3 3 1
IRAS 15534–5422	15 57 20.4	–54 30 40	25	6	106	1.06	8.27	12.41	355.80	3 3 2 1
IRAS 16209–4714	16 24 34.0	–47 21 29	21	4	96	1.17	18.87	20.68	63.87	3 3 3 1
IRAS 16228–5014	16 26 36.4	–50 21 05	13	5	146	0.79	25.68	66.78	159.60	3 3 3 1
IRAS 16245–3859	16 27 53.7	–39 05 46	43	9	99	3.78	25.27	31.62	16.13	3 3 3 3
IRAS 16279–8158	16 37 52.1	–82 04 49	11	4	102	4.21	10.31	5.70	2.35	3 3 3 3
IRAS 16296–4507	16 33 12.7	–45 13 44	17	3	97	3.26	17.67	14.20	31.32	3 3 3 1
IRAS 16333–4807	16 37 06.1	–48 13 42	17	4	97	9.33	42.98	89.26	113.20	3 3 3 1
IRAS 16507–4810	16 54 31.0	–48 15 21	33	11	99	1.08	12.56	8.96	13.48	3 2 2 2
IRAS 16517–3626	16 55 05.1	–36 31 30	34	5	100	1.51	5.97	2.27	11.38	3 3 3 1
IRAS 16518–3425	16 55 08.4	–34 30 10	24	6	120	1.02	7.98	1.66	5.16	3 3 3 1
IRAS 16558–3417	16 59 10.5	–34 22 05	30	6	98	2.63	11.60	7.68	10.85	3 3 3 2
IRAS 16559–2957	16 59 08.1	–30 01 40	19	5	98	9.17	32.37	16.38	4.19	3 3 3 1
IRAS 16567–3838	17 00 08.2	–38 43 08	40	5	99	7.30	15.68	7.07	58.57	3 3 3 1
IRAS 16584–3710	17 01 52.5	–37 14 57	38	6	99	0.91	6.14	4.39	25.12	3 3 3 1
IRAS 17009–4154	17 04 29.7	–41 58 35	33	6	99	7.44	86.38	65.84	260.00	3 3 3 1
IRAS 17010–3810	17 04 26.9	–38 14 43	24	6	99	2.23	14.78	7.68	30.04	3 3 3 1
IRAS 17021–3109	17 05 23.2	–31 13 18	37	5	97	3.29	11.97	16.59	7.88	3 3 3 3
IRAS 17021–3054	17 05 24.1	–30 58 13	23	5	97	1.18	5.34	2.49	16.78	3 3 3 1
IRAS 17052–3245	17 08 32.7	–32 49 43	35	6	97	3.13	10.79	12.02	10.12	3 3 3 1
IRAS 17067–3759	17 10 08.3	–38 03 22	29	6	98	1.98	10.60	10.66	68.33	3 3 3 1
IRAS 17088–4221	17 12 22.6	–42 25 13	26	5	98	42.70	128.30	106.80	36.90	3 3 3 3
IRAS 17097–3624	17 13 05.1	–36 27 54	42	6	97	1.52	6.62	10.11	227.40	3 3 3 1
IRAS 17149–3053	17 18 11.7	–30 56 40	36	6	96	2.13	11.12	7.82	20.93	3 3 3 1
IRAS 17150–3224	17 18 19.9	–32 27 20	32	6	96	57.92	322.30	268.30	82.41	3 3 3 3
IRAS 17153–3814	17 18 44.6	–38 17 23	15	4	97	2.64	19.55	52.88	436.50	3 3 3 1
IRAS 17158–4049	17 19 20.9	–40 52 43	46	6	97	0.99	6.56	7.14	295.40	3 3 3 1
IRAS 17168–3736	17 20 15.0	–37 39 32	18	5	97	9.79	36.98	47.89	280.60	3 3 3 1
IRAS 17175–2819	17 20 42.4	–28 22 36	42	5	95	3.38	14.94	5.23	10.18	3 3 3 1
IRAS 17233–2602	17 26 28.7	–26 04 58	27	5	94	3.69	10.61	7.19	7.93	3 3 3 1
IRAS 17234–4008	17 26 55.6	–40 11 03	37	6	96	1.48	12.46	10.48	83.69	3 3 3 1
IRAS 17269–2235	17 29 58.2	–22 37 34	26	7	93	0.68	14.89	22.26	8.85	2 3 3 3
IRAS 17291–2147	17 32 10.1	–21 49 59	24	6	93	2.54	12.18	8.24	6.42	3 3 3 1
IRAS 17301–2538	17 33 13.2	–25 40 24	20	5	93	0.78	7.80	4.29	33.13	3 3 3 1
IRAS 17348–2906	17 38 04.2	–29 08 23	39	9	93	4.71	11.55	8.24	305.50	3 3 3 1
IRAS 17359–2902	17 39 07.7	–29 04 02	41	9	93	2.04	12.38	7.61	259.60	3 3 2 1
IRAS 17360–2142	17 39 05.9	–21 43 52	25	7	92	0.93	12.53	12.46	6.52	3 3 3 1
IRAS 17361–4159	17 39 43.8	–42 00 41	25	5	95	2.58	6.73	5.54	24.89	3 3 3 1
IRAS 17376–3448	17 40 56.4	–34 50 03	22	5	93	3.70	10.18	6.92	13.33	3 3 3 1
IRAS 17382–2531	17 41 20.1	–25 32 53	38	5	92	3.03	7.64	5.31	11.46	3 3 3 1

**Table 1.** continued.

IRAS 17385-3332	17 41 52.2	-33 33 41	22	6	93	2.88	13.25	10.01	238.40	3 3 3 1
IRAS 17385-2413	17 41 38.3	-24 14 41	32	6	92	3.73	7.67	3.70	9.93	3 3 3 1
IRAS 17393-2727	17 42 32.2	-27 28 28	40	7	92	1.83	17.83	36.85	85.69	2 3 3 1
IRAS 17404-2713	17 43 39.4	-27 14 18	20	6	92	3.99	20.74	15.49	83.59	3 3 3 1
IRAS 17418-3335	17 45 10.7	-33 36 13	18	5	94	1.83	14.63	12.06	161.90	3 3 3 1
IRAS 17443-2949	17 47 35.2	-29 50 56	34	6	93	15.77	39.39	34.47	354.10	3 3 3 1
IRAS 17479-3032	17 51 12.5	-30 33 44	33	7	92	2.63	13.02	16.51	106.10	2 3 2 1
IRAS 17482-2501	17 51 22.3	-25 01 50	27	8	91	1.34	5.18	11.53	381.60	2 3 3 1
IRAS 17487-1922	17 51 44.7	-19 23 42	31	8	91	2.16	20.25	7.21	11.81	3 3 3 1
IRAS 17499-3520	17 53 19.7	-35 21 11	30	6	92	2.82	13.10	4.02	6.10	3 3 3 1
IRAS 17506-2955	17 53 49.3	-29 55 34	21	6	91	1.62	6.29	6.61	194.40	3 3 3 1
IRAS 17516-2525	17 54 43.5	-25 26 27	29	6	91	51.58	115.60	100.10	292.10	3 3 3 1
IRAS 17540-2753	17 57 14.1	-27 54 16	16	4	91	1.39	14.19	26.16	341.00	2 3 3 1
IRAS 17543-3102	17 57 34.2	-31 03 00	27	6	91	2.76	21.87	24.44	71.27	3 3 3 1
IRAS 17548-2753	17 57 57.7	-27 53 20	29	5	91	1.27	16.95	21.95	174.90	3 3 3 1
IRAS 17550-2800	17 58 10.6	-28 00 26	37	5	91	2.52	5.89	5.96	203.40	3 3 3 1
IRAS 17550-2120	17 58 04.9	-21 21 07	32	5	90	5.38	21.08	30.81	43.64	3 3 3 1
IRAS 17552-2030	17 58 16.3	-20 30 22	37	6	90	1.22	4.62	3.93	29.08	3 3 3 1
IRAS 17560-2027	17 59 04.4	-20 27 23	24	6	90	1.59	15.32	17.79	40.99	3 3 3 1
IRAS 17580-3111	18 01 19.7	-31 11 23	38	7	91	3.24	15.32	7.96	15.19	3 3 3 1
IRAS 17582-2619	18 01 21.2	-26 19 37	24	8	90	1.38	9.28	7.92	293.30	3 3 3 1
IRAS 17596-3952	18 03 06.2	-39 51 55	34	10	92	0.48	1.11	0.59	12.68	3 2 2 1
IRAS 18011-1847	18 04 02.7	-18 47 10	32	5	89	2.54	13.67	16.30	60.24	3 3 3 1
IRAS 18015-1352	18 04 22.2	-13 51 49	29	7	89	2.11	4.24	3.37	21.74	3 3 3 2
IRAS 18016-2743	18 04 45.8	-27 43 11	24	5	90	3.02	7.15	3.07	131.80	3 3 3 1
IRAS 18039-1903	18 06 53.3	-19 03 09	37	6	89	4.17	11.11	7.31	261.90	3 3 2 1
IRAS 18049-2118	18 07 54.8	-21 18 09	42	6	89	11.83	25.70	9.12	206.50	3 3 3 1
IRAS 18051-2415	18 08 12.8	-24 14 36	38	6	90	1.88	8.14	9.49	172.30	3 3 3 1
IRAS 18071-1727	18 10 05.4	-17 26 56	26	7	89	23.66	76.57	83.46	304.70	3 3 3 1
IRAS 18083-2155	18 11 18.9	-21 55 05	24	6	89	7.40	37.97	27.07	496.00	3 3 3 1
IRAS 18087-1440	18 11 34.2	-14 39 59	28	7	88	2.58	21.86	32.31	217.20	3 3 3 1
IRAS 18105-1935	18 13 32.2	-19 35 03	22	7	89	7.33	19.87	10.46	369.50	3 3 3 1
IRAS 18113-2503	18 14 26.2	-25 02 55	33	6	89	2.90	14.77	12.90	29.16	3 3 3 1
IRAS 18135-1456	18 16 25.6	-14 55 15	20	6	88	31.02	124.40	157.60	429.10	3 3 3 1
IRAS 18183-2538	18 21 24.7	-25 36 35	22	6	88	1.64	3.91	2.05	33.40	3 3 3 1
IRAS 18199-1442	18 22 50.8	-14 40 49	22	6	87	12.05	25.54	22.25	282.60	3 3 2 1
IRAS 18229-1127	18 25 45.0	-11 25 56	15	6	87	6.28	27.86	37.09	133.50	3 2 3 2
IRAS 18236-0447	18 26 20.3	-04 45 42	41	6	86	2.08	5.17	5.06	12.12	3 3 3 1
IRAS 18246-1032	18 27 24.0	-10 30 24	30	6	86	2.19	20.25	50.37	386.00	3 3 3 1
IRAS 18355-0712	18 38 15.4	-07 09 52	31	5	85	1.73	14.34	31.14	159.90	2 3 2 1
IRAS 18361-1203	18 38 58.8	-12 00 44	37	6	86	2.24	4.83	3.33	52.79	3 3 3 1
IRAS 18385+1350	18 40 52.0	+13 52 53	13	4	26	0.49	3.34	3.61	3.83	3 3 3 3
IRAS 18434-0042	18 46 04.4	-00 38 55	30	6	83	1.97	5.61	3.25	343.40	3 3 2 1
IRAS 18454+0001	18 48 01.5	+00 04 47	39	8	83	0.80	14.54	13.61	383.50	2 3 3 1
IRAS 18470+0015	18 49 39.1	+00 18 52	38	6	83	4.11	10.67	8.07	249.60	3 3 3 1
IRAS 18485+0642	18 50 58.9	+06 45 55	18	6	80	3.58	21.86	25.32	61.08	3 3 3 1
IRAS 18514+0019	18 53 57.9	+00 23 24	29	6	81	4.95	23.38	17.26	152.20	3 3 3 1
IRAS 18524+0544	18 54 54.1	+05 48 11	21	5	75	0.37	5.61	5.04	39.88	3 3 3 1
IRAS 18529+0210	18 55 26.3	+02 14 49	22	6	81	5.69	16.24	15.24	1921.00	3 3 3 1
IRAS 18576+0341	19 00 10.9	+03 45 47	23	5	81	58.48	425.00	274.70	1660.00	3 3 3 1
IRAS 18580+0818	19 00 25.2	+08 22 46	27	6	79	0.90	3.35	2.31	16.39	3 3 3 1
IRAS 18596+0315	19 02 06.2	+03 20 16	24	8	80	2.60	14.17	22.57	112.80	3 3 3 1
IRAS 19006+1022	19 02 59.9	+10 26 35	29	8	79	1.02	5.34	6.58	12.85	3 3 3 1
IRAS 19011+1049	19 03 30.7	+10 53 53	50	6	79	9.40	26.10	12.33	9.26	3 3 3 1
IRAS 19013+0629	19 03 44.4	+06 34 12	30	12	79	5.12	17.60	16.31	79.21	3 3 3 1
IRAS 19015+1256	19 03 52.6	+13 01 21	23	5	38	0.92	4.20	1.33	7.60	3 3 2 1
IRAS 19071+0857	19 09 29.7	+09 02 23	26	9	79	0.94	17.26	13.06	72.03	3 3 3 1
IRAS 19075+0432	19 10 00.0	+04 37 06	27	8	80	5.25	28.13	31.77	14.36	3 3 3 3
IRAS 19079-0315	19 10 32.4	-03 10 16	23	7	81	2.27	12.03	4.22	16.56	3 3 3 1
IRAS 19083+0119	19 10 54.4	+01 24 42	21	7	80	2.34	15.58	14.27	4.72	3 3 3 2
IRAS 19094+1627	19 11 44.5	+16 32 54	25	7	78	0.80	5.17	2.68	5.85	3 3 3 1
IRAS 19134+2131	19 15 35.4	+21 36 33	32	5	77	5.06	15.56	8.56	3.95	3 3 3 1
IRAS 19176+1251	19 19 55.8	+12 57 34	27	6	78	0.85	10.70	4.11	71.30	3 3 3 1
IRAS 19178+1206	19 20 14.0	+12 12 20	17	6	78	3.66	8.57	4.85	68.21	3 3 3 1
IRAS 19181+1806	19 20 25.2	+18 11 41	37	5	78	0.47	4.14	7.38	14.09	2 3 3 1
IRAS 19190+1102	19 21 25.3	+11 08 40	28	5	78	1.59	13.67	24.52	20.41	3 3 3 3
IRAS 19193+1804	19 21 31.5	+18 10 09	27	6	78	0.54	9.11	15.84	58.62	3 3 3 1
IRAS 19208+1541	19 23 06.8	+15 47 33	26	5	78	0.77	1.57	3.37	92.78	3 3 3 1
IRAS 19315+2235	19 33 41.6	+22 42 08	16	5	74	1.05	5.68	4.41	8.80	3 3 3 1
IRAS 19319+2214	19 34 03.5	+22 21 16	24	4	74	3.18	6.58	3.16	39.29	3 3 3 1
IRAS 19374+2359	19 39 35.6	+24 06 28	32	5	71	23.62	98.18	70.87	768.40	3 3 3 1
IRAS 19454+2920	19 47 24.2	+29 28 11	19	5	69	17.27	89.56	54.43	14.66	3 3 3 3
IRAS 20035+3242	20 05 29.6	+32 51 35	20	3	66	7.49	25.59	21.16	16.39	3 3 3 2
IRAS 20042+3259	20 06 10.6	+33 07 51	22	5	64	1.49	4.40	1.89	41.49	3 3 3 1
IRAS 20174+3222	20 19 28.0	+32 32 13	21	5	64	2.44	16.02	8.04	8.73	3 3 3 2
IRAS 20214+3749	20 23 19.2	+37 58 52	22	5	67	1.95	4.21	2.82	184.10	3 3 2 1
IRAS 20244+3509	20 26 25.4	+35 19 14	20	6	67	1.27	4.31	4.36	179.30	3 3 3 1
IRAS 20406+2953	20 42 45.9	+30 04 06	36	5	67	12.48	68.37	49.77	13.00	3 3 3 2
IRAS 20461+3853	20 48 04.6	+39 05 00	31	5	57	2.10	11.28	4.80	4.46	3 3 3 1
IRAS 21525+5643	21 54 15.0	+56 57 23	9	3	15	4.33	11.62	8.93	20.47	3 3 3 1
IRAS 21537+6435	21 55 04.5	+64 49 54	12	4	161	6.91	26.10	13.34	6.07	3 3 3 1
IRAS 21537+6435	21 55 04.5	+64 49 54	12	4	161	6.91	26.10	13.34	6.07	3 3 3 1
IRAS 21554+6204	21 56 58.1	+62 18 43	8	4	9	62.94	138.20	52.13	15.59	3 3 3 3

<sup>†</sup> The *IRAS* flux quality factor, FQUAL, indicates whether the flux values are of high quality (3), moderate quality (2), or simply represent an upper limit of the flux (1). The four values in this column refer consecutively to the flux quality in the 12  $\mu\text{m}$ , 25  $\mu\text{m}$ , 60  $\mu\text{m}$ , and 100  $\mu\text{m}$  bands.

**Table 2.** *IRAS* Post-AGB Star and PN Candidates with Near-IR Counterparts in the 2MASS PSC.

Object	$\alpha$ (J2000)	$\delta$ (J2000)	$\Delta\alpha$ ( $''$ )	$\Delta\delta$ ( $''$ )	Distance ( $''$ )	Optical	$J$ (mag)	$H$ (mag)	$K$ (mag)
IRAS 00509+6623	00 54 07.67	+66 40 12.8	-0.2	-0.2	0.3	Yes	13.950 $\pm$ 0.032	12.175 $\pm$ 0.032	10.634 $\pm$ 0.024
IRAS 08242-3828	08 26 03.78	-38 38 47.4	3.3	0.6	3.3	Yes	7.08 $\pm$ 0.04	5.68 $\pm$ 0.04	4.912 $\pm$ 0.022
IRAS 09055-4629	09 07 19.56	-46 41 23.6	1.6	-2.6	3.1	No	15.90 $\pm$ 0.08	14.14 $\pm$ 0.04	12.686 $\pm$ 0.032
IRAS 09102-5101	09 11 57.36	-51 14 24.9	36.3	-33.9	49.6	Yes	14.41 $\pm$ 0.05	13.88 $\pm$ 0.06	12.77 $\pm$ 0.05
IRAS 09119-5150	09 13 33.03	-52 02 41.6	1.2	-2.6	2.9	Yes	13.99 $\pm$ 0.04	13.18 $\pm$ 0.04	11.85 $\pm$ 0.04
IRAS 09378-5117	09 39 37.02	-51 31 29.3	1.1	-3.3	3.5	Yes	12.077 $\pm$ 0.026	10.876 $\pm$ 0.022	10.273 $\pm$ 0.021
IRAS 09500-5236	09 51 50.04	-52 50 52.1	4.9	-12.1	13.1	No	17.2	14.62 $\pm$ 0.06	11.845 $\pm$ 0.023
IRAS 11339-6004	11 36 20.69	-60 20 53.3	-2.3	2.7	3.5	No	15.30 $\pm$ 0.07	14.20 $\pm$ 0.07	13.64 $\pm$ 0.05
IRAS 11488-6432	11 51 17.36	-64 49 12.7	2.3	-3.7	4.4	Yes	10.907 $\pm$ 0.026	9.354 $\pm$ 0.024	8.325 $\pm$ 0.027
IRAS 12262-6417	12 29 04.49	-64 33 38.0	1.9	-1.0	2.1	Yes	12.53 $\pm$ 0.04	10.754 $\pm$ 0.029	9.150 $\pm$ 0.023
IRAS 12309-5928	12 33 44.58	-59 45 18.5	-1.7	-0.5	1.7	No	16.07 $\pm$ 0.11	13.843 $\pm$ 0.030	11.861 $\pm$ 0.025
IRAS 13356-6249	13 39 06.31	-63 04 44.3	3.5	-0.3	3.5	No	9.546 $\pm$ 0.024	8.00 $\pm$ 0.06	7.068 $\pm$ 0.024
IRAS 13398-5951	13 43 12.56	-60 07 03.5	2.7	-2.5	3.7	No	13.372 $\pm$ 0.027	11.813 $\pm$ 0.023	10.655 $\pm$ 0.021
IRAS 13421-6125	13 45 34.08	-61 40 03.8	-5.8	3.2	6.7	Yes	12.027 $\pm$ 0.026	10.835 $\pm$ 0.022	10.415 $\pm$ 0.023
IRAS 13483-5905	13 51 43.73	-59 20 15.5	-2.8	0.5	2.9	Yes	13.669 $\pm$ 0.021	12.800 $\pm$ 0.022	12.508 $\pm$ 0.021
IRAS 14104-5819	14 14 00.56	-58 33 58.0	1.3	-1.0	1.6	No	16.3	14.204 $\pm$ 0.09	10.690 $\pm$ 0.024
IRAS 14521-5300	14 55 45.70	-53 12 30.1	-1.8	2.9	3.4	Yes	11.042 $\pm$ 0.022	10.236 $\pm$ 0.023	9.876 $\pm$ 0.023
IRAS 15038-5533	15 07 34.77	-55 44 50.7	-5.3	3.3	6.3	No	15.04 $\pm$ 0.07	12.98 $\pm$ 0.04	11.784 $\pm$ 0.027
IRAS 15144-5812	15 18 21.92	-58 23 11.9	-0.6	1.1	1.3	Yes	11.066 $\pm$ 0.026	9.068 $\pm$ 0.023	7.348 $\pm$ 0.018
IRAS 15408-5657	15 44 48.36	-57 07 08.7	2.1	-0.7	2.2	No	17.4	15.3	11.519 $\pm$ 0.026
IRAS 15408-5413	15 44 39.80	-54 23 05.0	-0.9	0.0	0.9	No	7.583 $\pm$ 0.021	4.769 $\pm$ 0.015	3.07 $\pm$ 0.31
IRAS 16228-5014	16 26 34.27	-50 21 01.8	-20.4	3.2	20.6	Yes	9.927 $\pm$ 0.026	8.55 $\pm$ 0.05	7.735 $\pm$ 0.023
IRAS 16279-8158	16 37 51.63	-82 04 49.9	-1.0	-0.9	1.3	Yes	10.308 $\pm$ 0.023	9.263 $\pm$ 0.025	8.818 $\pm$ 0.023
IRAS 16517-3626	16 55 06.20	-36 31 32.2	13.3	-2.2	13.4	Yes	12.652 $\pm$ 0.026	11.900 $\pm$ 0.025	11.2
IRAS 16559-2957	16 59 08.22	-30 01 40.3	1.6	-0.3	1.6	Yes	11.596 $\pm$ 0.023	10.713 $\pm$ 0.023	9.347 $\pm$ 0.021
IRAS 16567-3838	17 00 09.07	-38 43 09.1	10.2	-1.1	10.2	No	15.9	14.7	11.632 $\pm$ 0.027
IRAS 16584-3710	17 01 52.05	-37 14 53.7	-5.4	3.3	6.3	No	16.5	14.00 $\pm$ 0.04	11.721 $\pm$ 0.025
IRAS 17010-3810	17 04 27.31	-38 14 41.7	4.8	1.3	5.0	Yes	13.110 $\pm$ 0.022	12.040 $\pm$ 0.028	11.302 $\pm$ 0.020
IRAS 17021-3109	17 05 23.71	-31 13 18.7	6.5	-0.7	6.6	No	17.4	16.4	13.88 $\pm$ 0.05
IRAS 17021-3054	17 05 23.83	-30 58 13.0	-3.5	0.0	3.5	No	14.61 $\pm$ 0.08	12.91 $\pm$ 0.06	11.532 $\pm$ 0.034
IRAS 17149-3053	17 18 10.93	-30 56 39.9	-9.9	0.1	9.9	No	15.8	14.5	13.37 $\pm$ 0.06
IRAS 17175-2819	17 18 19.85	-32 27 21.6	-0.9	-1.4	1.7	Yes	11.10 $\pm$ 0.04	10.22 $\pm$ 0.04	9.391 $\pm$ 0.024
IRAS 17233-2602	17 26 28.99	-26 04 56.8	3.9	1.2	4.1	Yes	14.93 $\pm$ 0.04	13.88 $\pm$ 0.04	13.10 $\pm$ 0.04
IRAS 17291-2147	17 32 11.17	-21 50 02.2	14.9	-3.2	15.2	Yes	13.507 $\pm$ 0.021	12.188 $\pm$ 0.022	11.008 $\pm$ 0.019
IRAS 17348-2906	17 38 03.92	-29 08 16.5	-3.7	6.5	7.5	Yes	8.027 $\pm$ 0.023	6.302 $\pm$ 0.047	5.395 $\pm$ 0.018
IRAS 17359-2902	17 39 07.70	-29 04 02.8	-0.1	0.1	0.2	No	12.75 $\pm$ 0.06	11.32 $\pm$ 0.07	10.44 $\pm$ 0.04
IRAS 17360-2142	17 39 05.95	-21 43 51.4	0.7	0.6	0.9	Yes	10.825 $\pm$ 0.023	9.714 $\pm$ 0.022	9.107 $\pm$ 0.019
IRAS 17385-3332	17 41 52.28	-33 33 40.6	1.0	0.4	1.1	Yes	10.484 $\pm$ 0.029	9.528 $\pm$ 0.030	9.018 $\pm$ 0.029
IRAS 17499-3520	17 53 20.42	-35 21 10.3	8.8	0.7	8.8	Yes	10.663 $\pm$ 0.024	10.005 $\pm$ 0.027	9.595 $\pm$ 0.019
IRAS 17516-2525	17 54 43.35	-25 26 28.0	-2.0	-1.0	2.3	Yes	8.695 $\pm$ 0.020	6.850 $\pm$ 0.036	5.082 $\pm$ 0.016
IRAS 17540-2753	17 57 11.41	-27 54 19.0	-35.7	-3.0	35.8	No	12.326 $\pm$ 0.028	10.903 $\pm$ 0.029	9.996 $\pm$ 0.021
IRAS 17548-2753	17 57 58.27	-27 53 20.2	7.6	-0.2	7.6	No	15.3	12.78 $\pm$ 0.04	11.465 $\pm$ 0.032
IRAS 17550-2800	17 58 09.57	-28 00 25.3	-13.6	0.7	13.7	Yes	12.5	11.04 $\pm$ 0.06	8.9
IRAS 17580-3111	18 01 20.40	-31 11 20.3	9.0	2.7	9.4	No	12.402 $\pm$ 0.024	10.551 $\pm$ 0.022	9.280 $\pm$ 0.019
IRAS 17582-2619	18 01 21.57	-26 19 37.3	5.0	-0.3	5.0	No	15.3	12.527 $\pm$ 0.030	10.840 $\pm$ 0.025
IRAS 17596-3952	18 03 06.77	-39 51 53.8	6.6	1.2	6.7	Yes	9.624 $\pm$ 0.026	8.845 $\pm$ 0.026	8.410 $\pm$ 0.022
IRAS 18015-1352	18 04 22.66	-13 51 50.1	6.7	-1.1	6.8	No	16.2	15.0	13.289 $\pm$ 0.035
IRAS 18049-2118	18 07 55.12	-21 18 08.3	4.5	0.7	4.5	No	16.6	13.9	11.312 $\pm$ 0.035
IRAS 18071-1727	18 10 06.07	-17 26 34.5	9.6	21.5	23.5	No	15.9	14.1	12.71 $\pm$ 0.06
IRAS 18105-1935	18 13 29.92	-19 35 02.9	-32.2	0.1	32.2	No	11.3	10.81 $\pm$ 0.04	9.2
IRAS 18113-2503	18 14 27.26	-25 03 00.4	14.4	-5.4	15.4	Yes	11.630 $\pm$ 0.033	10.698 $\pm$ 0.034	10.323 $\pm$ 0.030
IRAS 18183-2538	18 21 24.49	-25 36 35.0	-2.8	0.0	2.8	Yes	14.59 $\pm$ 0.04	13.043 $\pm$ 0.026	11.344 $\pm$ 0.023
IRAS 18199-1442	18 22 50.92	-14 40 48.3	1.7	0.7	1.9	No	16.9	15.8	11.146 $\pm$ 0.023
IRAS 18229-1127	18 25 41.49	-11 26 14.5	-51.6	-18.5	54.8	Yes	12.416 $\pm$ 0.029	11.39 $\pm$ 0.04	10.696 $\pm$ 0.029
IRAS 18236-0447	18 26 19.56	-04 45 44.3	-11.1	-2.3	11.3	No	16.5	15.30 $\pm$ 0.11	13.10 $\pm$ 0.04
IRAS 18355-0712	18 38 15.46	-07 09 54.3	0.9	-2.3	2.5	No	15.85 $\pm$ 0.11	13.12 $\pm$ 0.04	11.528 $\pm$ 0.035
IRAS 18361-1203	18 38 59.12	-12 00 42.0	4.7	2.0	5.1	Yes	11.727 $\pm$ 0.026	10.627 $\pm$ 0.032	10.027 $\pm$ 0.024
IRAS 18434-0042	18 46 04.70	-00 38 54.4	4.5	0.6	4.5	No	16.13 $\pm$ 0.10	13.806 $\pm$ 0.028	12.573 $\pm$ 0.022
IRAS 18454+0001	18 48 01.18	+00 04 48.5	-4.8	1.5	5.0	Yes	14.061 $\pm$ 0.026	12.876 $\pm$ 0.024	12.112 $\pm$ 0.025
IRAS 18470+0015	18 49 38.91	+00 18 54.9	-2.9	2.9	4.1	No	14.077 $\pm$ 0.13	12.454 $\pm$ 0.021	10.765 $\pm$ 0.020
IRAS 18485+0642	18 50 59.60	+06 45 59.0	10.4	4.0	11.2	Yes	14.020 $\pm$ 0.030	12.949 $\pm$ 0.031	12.325 $\pm$ 0.029
IRAS 18524+0544	18 54 54.14	+05 48 11.2	0.0	-0.1	0.1	Yes	14.58 $\pm$ 0.04	13.70 $\pm$ 0.04	12.412 $\pm$ 0.033
IRAS 18576+0341	19 00 10.89	+03 45 47.1	-0.2	0.1	0.2	No	12.164 $\pm$ 0.027	8.918 $\pm$ 0.028	7.007 $\pm$ 0.020
IRAS 19006+1022	19 03 00.03	+10 26 36.8	1.9	1.8	2.6	No	16.34 $\pm$ 0.13	13.55 $\pm$ 0.04	11.440 $\pm$ 0.023
IRAS 19075+0432	19 09 59.92	+04 37 08.5	-1.2	2.5	2.8	Yes	10.973 $\pm$ 0.021	10.061 $\pm$ 0.024	8.745 $\pm$ 0.025
IRAS 19079-0315	19 10 32.66	-03 10 13.0	3.9	3.0	4.9	Yes	11.979 $\pm$ 0.023	11.205 $\pm$ 0.025	10.588 $\pm$ 0.023
IRAS 19083+0119	19 10 54.53	+01 24 45.0	1.9	3.0	3.6	No	16.9	15.5	14.34 $\pm$ 0.08
IRAS 19094+1627	19 11 44.68	+16 32 55.4	2.6	1.4	2.9	Yes	12.829 $\pm$ 0.033	11.8	11.1
IRAS 19134+2131	19 15 35.20	+21 36 34.0	-2.8	1.0	3.0	No	16.54 $\pm$ 0.13	14.93 $\pm$ 0.07	13.46 $\pm$ 0.04
IRAS 19176+1251	19 19 55.77	+12 57 38.2	-0.4	4.2	4.2	No	16.04 $\pm$ 0.09	14.52 $\pm$ 0.05	13.020 $\pm$ 0.026
IRAS 19181+1806	19 20 24.86	+18 11 41.4	-4.8	0.4	4.9	Yes	13.472 $\pm$ 0.025	12.086 $\pm$ 0.018	10.984 $\pm$ 0.020
IRAS 19193+1804	19 21 31.63	+18 10 09.5	1.9	0.5	1.9	No	18.0	15.56 $\pm$ 0.13	14.29 $\pm$ 0.07
IRAS 19319+2214	19 34 03.58	+22 21 15.9	0.0	-0.1	0.1	No	13.668 $\pm$ 0.024	12.003 $\pm$ 0.022	10.747 $\pm$ 0.018

**Table 3.** *IRAS* Post-AGB Star and PN Candidates with no Counterparts in the 2MASS PSC.

Object	Optical	Comments
IRAS 04137+7016	Yes	Two objects unresolved by 2MASS.
IRAS 05573+3156	No	Diffuse emission.
IRAS 06499+0145	Yes	Diffuse emission.
IRAS 11381–6401	Yes	Two objects unresolved by 2MASS.
IRAS 11544–6408	Yes	Source very faint. 2MASS magnitudes not available.
IRAS 12360–5740	Yes	2MASS magnitudes contaminated by a nearby star.
IRAS 12405–6219	No	Diffuse emission or multiple objects unresolved by 2MASS.
IRAS 13293–6000	No	Two objects unresolved by 2MASS.
IRAS 13427–6531	Yes	Multiple objects unresolved by 2MASS.
IRAS 13529–5934	Yes	Two objects unresolved by 2MASS.
IRAS 14249–5310	No	Two objects unresolved by 2MASS.
IRAS 15103–5754	No	Diffuse emission.
IRAS 15229–5433	Yes	Diffuse emission or multiple objects unresolved by 2MASS.
IRAS 15452–5459	No	Diffuse emission.
IRAS 15534–5422	Yes	Diffuse emission.
IRAS 16209–4714	Yes	2MASS magnitudes contaminated by a nearby star.
IRAS 16296–4507	Yes	Diffuse emission or two objects unresolved by 2MASS.
IRAS 16333–4807	No	Diffuse emission.
IRAS 16507–4810	Yes	Diffuse emission or two objects unresolved by 2MASS.
IRAS 17009–4154	No	Diffuse emission.
IRAS 17052–3245	No	Source very faint. 2MASS magnitudes not available.
IRAS 17150–3224	Yes	Diffuse emission, the Cotton Candy Nebula.
IRAS 17234–4008	No	Two objects unresolved by 2MASS.
IRAS 17269–2235	Yes	Two objects unresolved by 2MASS.
IRAS 17301–2538	Yes	Two objects unresolved by 2MASS.
IRAS 17361–4159	No	Two objects unresolved by 2MASS.
IRAS 17376–3448	No	Diffuse emission or multiple objects unresolved by 2MASS.
IRAS 17418–3335	No	Two objects unresolved by 2MASS.
IRAS 17479–3032	No	Two objects unresolved by 2MASS.
IRAS 17487–1922	Yes	Two objects unresolved by 2MASS.
IRAS 17506–2955	No	Two objects unresolved by 2MASS.
IRAS 17560–2027	Yes	Two objects unresolved by 2MASS.
IRAS 18087–1440	No	Two objects unresolved by 2MASS.
IRAS 19015+1256	No	Two objects unresolved by 2MASS.
IRAS 19071+0857	No	Diffuse emission or multiple objects unresolved by 2MASS.
IRAS 19178+1206	No	Two objects unresolved by 2MASS.
IRAS 19208+1541	No	Two objects unresolved by 2MASS.
IRAS 20035+3242	No	Two objects unresolved by 2MASS.
IRAS 21554+6204	No	Two objects unresolved by 2MASS.

**Table 4.** *IRAS* Post-AGB Star and PN Candidates Without 2MASS Near-IR Counterparts.

IRAS 08351–4634	IRAS 15531–5704	IRAS 17158–4049	IRAS 17543–3102	IRAS 18135–1456	IRAS 19011+1049
IRAS 09370–4826	IRAS 16245–3859	IRAS 17168–3736	IRAS 17550–2120	IRAS 18246–1032	IRAS 19013+0629
IRAS 10194–5625	IRAS 16518–3425	IRAS 17382–2531	IRAS 17552–2030	IRAS 18385+1350	IRAS 19190+1102
IRAS 11444–6150	IRAS 16558–3417	IRAS 17385–2413	IRAS 18011–1847	IRAS 18514+0019	IRAS 19315+2235
IRAS 11549–6225	IRAS 17067–3759	IRAS 17393–2727	IRAS 18016–2743	IRAS 18529+0210	IRAS 19454+2920
IRAS 13404–6059	IRAS 17088–4221	IRAS 17404–2713	IRAS 18039–1903	IRAS 18580+0818	IRAS 20042+3259
IRAS 13500–6106	IRAS 17097–3624	IRAS 17443–2949	IRAS 18051–2415	IRAS 18596+0315	IRAS 21537+6435
IRAS 15284–6026	IRAS 17153–3814	IRAS 17482–2501	IRAS 18083–2155		

**Table 5.** *Spitzer* and *MSX* Fluxes of *IRAS* Post-AGB Star and PN Candidates with Counterparts in the 2MASS PSC.

	Spitzer				MSX			
	3.6 $\mu\text{m}$ [Jy]	4.5 $\mu\text{m}$ [Jy]	5.8 $\mu\text{m}$ [Jy]	8 $\mu\text{m}$ [Jy]	8.28 $\mu\text{m}$ [Jy]	12.13 $\mu\text{m}$ [Jy]	14.65 $\mu\text{m}$ [Jy]	21.3 $\mu\text{m}$ [Jy]
IRAS 00509+6623	...	...	...	...	1.18±0.05	2.75±0.19	2.45±0.18	3.50±0.27
IRAS 08242-3828	...	...	...	...	8.9±0.4	11.3±0.6	12.9±0.8	20.7±1.2
IRAS 09055-4629	...	...	...	...	0.26±0.01	0.78±0.05	0.86±0.06	1.98±0.13
IRAS 09102-5101	...	...	...	...	0.14±0.01	...	1.06±0.08	1.63±0.13
IRAS 09119-5150	...	...	...	...	0.30±0.02	1.05±0.09	1.26±0.09	2.14±0.16
IRAS 09500-5236	...	...	...	...	0.23±0.01	...	0.88±0.07	...
IRAS 09378-5117	...	...	...	...	0.76±0.03	2.17±0.13	3.89±0.24	4.92±0.31
IRAS 11339-6004	...	...	...	...	0.67±0.03	2.37±0.14	3.28±0.21	5.65±0.35
IRAS 11488-6432	...	...	...	...	1.03±0.04	1.49±0.10	1.72±0.11	2.02±0.15
IRAS 11544-6408	...	...	...	...	10.34±0.42	24.6±1.2	34.1±2.1	34.0±2.0
IRAS 12262-6417	...	...	...	...	1.86±0.08	2.55±0.15	2.64±0.17	5.01±0.32
IRAS 12309-5928	...	...	...	...	1.31±0.05	2.00±0.12	2.34±0.15	3.90±0.25
IRAS 13356-6249	...	...	0.747±0.022	0.882±0.030	1.49±0.06	7.6±0.4	22.1±1.4	103±6
IRAS 13398-5951	...	...	...	...	1.57±0.06	2.70±0.15	3.37±0.21	4.81±0.30
IRAS 13421-6125	0.273±0.031	...	...	...	7.14±0.29	14.6±0.7	22.4±1.4	22.0±1.3
IRAS 13483-5905	...	...	...	...	1.07±0.04	4.45±0.23	10.0±0.6	10.8±0.7
IRAS 14104-5819	...	...	...	...	3.64±0.15	4.59±0.24	7.8±0.5	9.2±0.6
IRAS 15038-5533	...	...	...	...	0.63±0.03	1.25±0.09	1.61±0.11	2.15±0.16
IRAS 15144-5812	0.35±0.07	3.35±0.21	4.41±0.11	...	5.13±0.21	6.53±0.33	8.8±0.5	26.6±1.6
IRAS 15408-5657	...	...	...	...	65.9±2.7	102±5	112±7	123±7
IRAS 15408-5413	...	...	...	...	135±6	231±12	257±16	298±18
IRAS 16228-5014	...	...	0.690±0.020	0.463±0.011	0.22±0.01	0.76±0.07	1.35±0.09	11.4±0.7
IRAS 16517-3626	...	...	...	...	0.75±0.03	1.65±0.13	2.39±0.16	5.45±0.35
IRAS 16518-3425	...	...	...	...	0.35±0.02	...	1.95±0.14	6.7±0.4
IRAS 16567-3838	...	...	...	...	5.88±0.24	8.5±0.4	11.1±0.7	13.4±0.8
IRAS 16584-3710	...	...	...	...	0.43±0.02	0.95±0.10	1.96±0.13	4.00±0.26
IRAS 17010-3810	...	...	...	...	0.55±0.02	2.21±0.13	4.08±0.25	8.2±0.5
IRAS 17021-3109	...	...	...	...	1.06±0.05	2.99±0.21	6.3±0.4	9.1±0.6
IRAS 17021-3054	...	...	...	...	0.42±0.02	...	3.32±0.23	4.51±0.32
IRAS 17149-3053	...	...	...	...	0.41±0.02	2.02±0.13	3.93±0.25	8.2±0.5
IRAS 17175-2819	...	...	...	...	12.7±0.5	61±3	128±8	247±15
IRAS 17233-2602	...	...	...	...	1.94±0.08	4.32±0.23	7.4±0.5	7.9±0.5
IRAS 17348-2906	...	...	2.54±0.07	...	1.92±0.08	3.30±0.18	3.92±0.24	7.7±0.5
IRAS 17359-2902	0.0520±0.0020	0.0522±0.0017	0.0610±0.0024	0.261±0.007	0.44±0.02	1.70±0.11	3.27±0.21	10.0±0.6
IRAS 17360-2142	...	...	...	...	0.26±0.01	1.3±0.6	2.31±0.15	8.9±0.5
IRAS 17385-3332	...	...	...	...	0.19±0.01	0.73±0.08	1.78±0.12	7.7±0.5
IRAS 17499-3520	...	...	...	...	0.76±0.03	2.40±0.15	3.65±0.23	10.3±0.6
IRAS 17516-2525	...	...	...	...	40.5±1.7	43.9±2.2	44.7±2.7	89±5
IRAS 17540-2753	0.0590±0.0020	0.0483±0.0027	0.0580±0.0018	0.292±0.010	0.38±0.02	1.41±0.10	3.74±0.24	10.0±0.6
IRAS 17548-2753	0.0367±0.0015	0.0462±0.0019	0.0480±0.0014	0.136±0.004	0.23±0.01	1.00±0.09	3.60±0.23	11.4±0.7
IRAS 17550-2800	...	...	1.90±0.06	...	2.29±0.09	2.17±0.13	3.00±0.19	4.28±0.28
IRAS 17580-3111	...	...	...	...	1.24±0.05	3.62±0.18	6.9±0.4	13.2±0.8
IRAS 17582-2619	...	...	...	...	0.38±0.02	1.65±0.11	3.45±0.22	7.0±0.4
IRAS 18015-1352	...	...	...	...	1.46±0.06	2.39±0.14	2.48±0.16	3.42±0.22
IRAS 18049-2118	...	3.90±0.34	11.4±0.8	...	8.31±0.34	13.4±0.7	17.6±1.1	18.3±1.1
IRAS 18071-1727	0.147±0.006	...	...	...	8.22±0.34	28.7±1.4	51.5±3.1	57.5±3.5
IRAS 18105-1935	0.370±0.021	...	2.22±0.05	4.32±0.11	3.78±0.15	8.3±0.4	12.0±0.7	15.0±0.9
IRAS 18113-2503	...	...	...	...	0.69±0.03	2.53±0.14	5.48±0.33	9.6±0.6
IRAS 18199-1442	0.542±0.04	2.83±0.15	...	...	15.7±0.6	22.3±1.1	29.8±1.8	28.4±1.7
IRAS 18229-1127	0.0368±0.0029	0.0434±0.0024	0.161±0.007	0.515±0.04	0.50±0.02	1.18±0.09	1.92±0.12	17.4±1.1
IRAS 18236-0447	...	...	...	...	0.67±0.03	1.40±0.10	2.70±0.17	2.73±0.19
IRAS 18355-0712	0.0416±0.0019	0.0689±0.0019	0.1011±0.0021	0.227±0.004	0.27±0.01	1.55±0.08	3.86±0.24	9.4±0.6
IRAS 18361-1203	...	...	...	...	1.57±0.06	2.63±0.15	3.29±0.21	4.31±0.27
IRAS 18434-0042	0.0078±0.0004	0.0113±0.0007	0.0266±0.0010	0.1249±0.0031	0.14±0.01	0.62±0.07	1.48±0.10	2.81±0.18
IRAS 18454+0001	0.0105±0.0004	0.0106±0.0003	0.0319±0.0009	0.099±0.004	0.12±0.01	0.41±0.03	1.24±0.08	9.5±0.6
IRAS 18470+0015	0.216±0.009	0.447±0.018	0.807±0.022	...	2.15±0.09	4.64±0.23	6.1±0.4	8.8±0.5
IRAS 18485+0642	...	...	...	...	0.99±0.04	3.42±0.18	7.8±0.5	14.9±0.9
IRAS 18524+0544	...	...	...	...	0.19±0.01	...	1.44±0.10	3.43±0.22
IRAS 18576+0341	2.3±0.4	...	...	...	10.6±0.4	45.5±2.3	89±5	277±17
IRAS 19006+1022	...	...	...	...	0.56±0.02	...	1.47±0.10	2.93±0.20
IRAS 19075+0432	...	...	...	...	4.51±0.19	5.34±0.27	8.6±0.5	17.0±1.0
IRAS 19083+0119	...	...	...	...	0.54±0.02	2.18±0.13	5.08±0.31	11.1±0.7
IRAS 19094+1627	...	...	...	...	0.32±0.02	0.75±0.08	1.34±0.10	2.40±0.17
IRAS 19134+2131	...	...	...	...	1.22±0.05	5.06±0.27	8.9±0.5	10.1±0.6
IRAS 19176+1251	0.0071±0.0003	0.0124±0.0005	0.0189±0.0006	0.162±0.005	0.32±0.01	1.13±0.08	2.06±0.13	8.1±0.5
IRAS 19181+1806	...	...	...	...	0.22±0.01	...	0.80±0.07	2.63±0.18
IRAS 19193+1804	...	...	...	...	0.11±0.01	...	1.95±0.13	5.17±0.32
IRAS 19319+2214	...	...	...	...	2.23±0.09	3.52±0.19	4.82±0.30	5.27±0.33
IRAS 19374+2359	0.430±0.011	...	...	...	13.8±0.6	23.72±1.19	33.7±2.1	68±4
IRAS 20174+3222	...	...	...	...	0.87±0.04	2.81±0.16	3.32±0.21	11.5±0.7
IRAS 20214+3749	...	...	...	...	1.23±0.05	1.93±0.12	2.18±0.14	2.60±0.18
IRAS 20244+3509	...	...	...	...	0.76±0.03	1.08±0.09	1.53±0.11	3.03±0.20
IRAS 20461+3853	...	...	...	...	0.82±0.03	2.48±0.14	3.01±0.19	6.8±0.4
IRAS 21525+5643	...	...	...	...	2.28±0.09	5.25±0.27	6.8±0.4	9.9±0.6

# **Online Material**

**Fig. 3.** (*left*) 2MASS  $J$  (blue),  $H$  (green), and  $K_S$  (red) composite pictures and (*right*) IR spectral energy distributions (SEDs) of the *IRAS* post-AGB star and PN candidates with near-IR counterparts in the 2MASS PSC. In the pictures, north is up, east to the left, and the locations of the near-IR counterparts and their type (*o* or *n* whether they are detected in DSS red images or not) are overlaid. The SEDs are built using data extracted from the 2MASS, *Spitzer* GLIMPSE, MSX, and *IRAS* catalogues. The arrows at  $100\ \mu\text{m}$  represent flux upper limits (IRAS quality factor, FQUAL, equals to 1).

**Fig. 4.** 2MASS  $J$  (blue),  $H$  (green), and  $K_S$  (red) composite pictures of the *IRAS* post-AGB star and PN candidates with near-IR counterparts that are not resolved or clearly detected in the 2MASS PSC. The locations of the near-IR counterparts and their type (*o* or *n* whether they are detected in DSS red images or not) are overlaid on the pictures. North is up, east to the left.

**Fig. 8.** *Spitzer* GLIMPSE composite pictures of the *IRAS* post-AGB star and PN candidates with near-IR counterparts in the 2MASS PSC and *Spitzer* observations. The blue, green, and red colours in the composite pictures correspond to the  $3.6\ \mu\text{m}$ ,  $4.5\ \mu\text{m}$ , and  $8.0\ \mu\text{m}$  bands, respectively, except for the pictures of IRAS 13421–6125, IRAS 15408–5413, IRAS 19374+2359, and IRAS 18576+0341 where they represent the  $3.6\ \mu\text{m}$ ,  $4.5\ \mu\text{m}$ , and  $5.8\ \mu\text{m}$  bands, respectively, and for the picture of IRAS 17548–2753 where the  $4.5\ \mu\text{m}$  band is shown in blue and green, and the  $8.0\ \mu\text{m}$  band is shown in red. The locations of the sources are overlaid on the pictures. North is up, east to the left.